Separation and Purification Technology 312 (2023) 123373

Contents lists available at ScienceDirect

Separation and Purification Technology

journal homepage: www.elsevier.com/locate/seppur

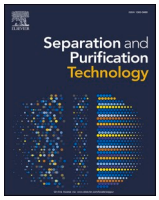

Separation of tripeptides in binary mixtures using ion-exchange membrane adsorber

Jordi Labanda *, Joan Llorens

Department of Chemical Engineering and Analytical Chemistry, University of Barcelona, Martí i Franquès 1, 08028 Barcelona, Spain

ARTICLE INFO

Keywords:
Triglycine
Competitive adsorption
Modified Langmuir isotherm
Axial dispersion
Peptide recovery

ABSTRACT

The adsorption of three tripeptides in an ion-exchange membrane adsorber was analyzed in single and binary solutions, with the aim of evaluating the capability of the membrane adsorber to separate triglycine (GGG) from two other tripeptides: glycine-histidine-glycine (GHG) and glycine-tyrosine-glycine (GTG). The equilibrium adsorption of single peptide solutions followed the Langmuir isotherm and GTG showed the highest adsorption affinity. The dynamic adsorption was fitted with a generalized model, which was defined using dimensionless parameters and based on the continuity equation. In general, the calculated and experimental breakthrough curves were correlated with high agreement. It was found that the axial dispersion coefficient was independent of the peptide molecule and that it increased with flow rate. The competitive adsorption between peptides in binary solutions was analyzed using the extended and modified Langmuir equations. The adsorption equilibrium data were satisfactorily fitted with the modified Langmuir isotherm for GGG/GHG solutions, while the extended Langmuir isotherm was a better fit to the data for GGG/GTG solutions. The experimental breakthrough curves of the two peptide binary mixtures were simulated using the parameters calculated from the competitive isotherms and the parameters obtained from the breakthrough curves of the single peptide solutions. The separation of GGG from the GGG/GHG mixtures was possible. The GGG recovery was higher than 35% and the GGG molar fraction in the outlet stream was higher than 0.994.

1. Introduction

Biomolecules such as amino acids, peptides and proteins are industrially important and of great interest in the food technology and pharmaceutical industries. Small peptides, formed by two or three amino acids (called dipeptides and tripeptides, respectively), are present in most downstream processes and aqueous washing streams in food processing of potato starch, sugar, vegetable canning and in other agro industries, and also form part of the streams derived from food protein hydrolysates [1]. These molecules are valuable ingredients for the food industry when they are free of other organic molecules such as polysaccharides and inorganic salts. Moreover, peptides are found at low concentrations in all industrial streams. For these reasons, the separation and purification of peptides is a complex process that needs highly selective separation technologies to ensure their efficient isolation [2].

Several separation technologies can be used to purify and separate peptides. Among the pressure-drive membrane technologies, which are generally not able to separate molecules with similar molecular weights, adsorption onto specific binding sites is the most commonly used. Conventionally, resin-based adsorption columns have been used for the isolation and purification of biomolecules. Several different types of adsorbents have shown high binding capacity for peptides. The main adsorbents used are formed by microporous inorganic solids, such as clays [3–5], zeolites [6,7], and activated carbon [8,9]. However, the adsorption of peptides onto several polymeric resins [10,11] and, recently, onto metal–organic sorbents [12] has also been studied. Wijntje *et al.* (2007) analyzed the adsorption of tripeptides in several types of sorbents and found that zeolites showed the best results [7]. Currently, new adsorbents are being developed to improve their adsorption capacity, although as yet only their ability to retain contaminants in wastewater has been tested [13–15]. Promising results in peptide adsorption are now expected.

The main limitations of conventional adsorption are the low volumetric flow rates and the large drop in pressure across the resin-packed bed. The diffusion of solute molecules inside the micropores is the main mechanism of adsorption to find the binding sites [16–18]. One alternative to resin-based adsorption processes involves the use of membrane adsorbers, which combine the selectivity of chromatography adsorption and the productivity of membranes [19]. The main advantages of

* Corresponding author.
E-mail address: jlabanda@ub.edu (J. Labanda).

https://doi.org/10.1016/j.seppur.2023.123373
Received 24 November 2022; Received in revised form 30 January 2023; Accepted 4 February 2023
Available online 14 February 2023

Nomenclature

b_i	constant of Langmuir isotherm (L/mol)
c_i	solute concentration in the liquid phase (mol/L)
c_{ieq}	equilibrium solute concentration in the liquid-phase (mol/L)
c_{ci}	cumulative solute concentration in the outlet stream (mol/L)
c_{sb}	breakthrough adsorption capacity (mol/L)
c_{si}	adsorbed solute concentration in the solid phase (mol/L)
c^*_{Es}	maximum adsorbed solute concentration in the solid phase for extended Langmuir equation (mol/L)
c^*_{si}	maximum adsorbed solute concentration in the solid phase (mol/L)
c_{si_eq}	equilibrium solute concentration in the solid phase (mol/L)
$c_{si\_eq\_o}$	equilibrium feed solute concentration in the solid phase (mol/L)
c_{ss}	Saturated adsorption capacity (mol/L)
C_i	dimensionless solute concentration in the liquid phase
C_{ieq}	dimensionless equilibrium solute concentration in the liquid phase
C_{si}	dimensionless adsorbed solute concentration in the solid phase
C_{si_eq}	dimensionless equilibrium solute concentration in the solid phase
D_{Li}	axial dispersion coefficient (m^2/s)
k_{ai}	adsorption rate constant ($L/mol\ s^{-1}$)
k_{di}	desorption rate constant (s^{-1})
k_{Eai}	adsorption rate constant of extended Langmuir equation ($L/mol\ s^{-1}$)
k_{Edi}	desorption rate constant of extended Langmuir equation ($L/mol\ s^{-1}$)
$K_{ads,i}$	dimensionless adsorption constant
L	membrane thickness (m)
m_i	dimensionless ratio between the equilibrium solute concentration in the solid phase and the feed solute concentration
p_i	dimensionless ratio between the equilibrium feed solute concentration in the solid-phase and the maximum possible concentration of adsorbed solute in the solid-phase
Pe_i	axial Peclet number
r_i	Dimensionless ratio between adsorption and desorption constants
t	time (s)
$t_{ads,i}$	characteristic time related to adsorption process (s)
t_b	breakthrough time (s)
$t_{des,i}$	characteristic time related to desorption process (s)
$t_{disp,i}$	characteristic time related to axial dispersion (s)
$t_{process}$	convective time or characteristic time of the process (s)
t_s	saturated time (s)
v	flow velocity (m/s)
V_{b2}	volume in the outlet stream corresponding to the breakthrough point (mL)
X_s	molar fraction adsorbed to the solid phase
Z	axial distance along the membrane (m)

Greek letters

ε	porosity of membrane
η	parameter of modified Langmuir equation
μ	viscosity of water (mPa·s)
τ	dimensionless time
ζ	dimensionless spatial variable

membrane adsorbers are the absence of long diffusive pathways and the use of high volumetric flow rates, which mean that adsorption performed with membrane adsorbers is faster than a traditional column configuration [20]. Hence, solutes can reach the binding sites more quickly and the residence time is reduced. Two different configurations are available in membrane adsorbers: axial and radial. The main difference between these configurations is the low fluid velocity in radial devices, which increases the residence time and the adsorption effectiveness compared with axial devices [21]. The more extended membrane matrix type includes ion-exchange and affinity membrane adsorbers, which have been used to study the adsorption of valuable biomolecules [20,22–24].

Modeling of the adsorption process in a membrane adsorber is based on the continuity equation, the kinetic adsorption rate equation, and the isotherm equation [25–28]. The continuity equation is based on the differential mass balance, which considers the time derivation of solute concentration in the liquid phase, the axial convective flux, the solute movement through the membrane, and the adsorption to binding sites situated on the membrane surface. A redefinition of the continuity equation with dimensionless parameters has been proposed by defining characteristic times that quantify axial convection, axial dispersion and the adsorption and desorption process [25,29]. The most commonly used kinetic adsorption rate equation is based on simultaneous adsorption and desorption processes, which are assumed to be a function of free binding sites and solute adsorbed on the solid phase, respectively. Under steady state conditions, the isotherm equation quantifies the adsorption process. The simplest isotherms are the well-known Langmuir equation, which assumes energetic homogeneity of the adsorption sites without steric effects, and the Freundlich equation, which assumes non-homogenous adsorption [30,31]. Modifications of these isotherms have also been used to better quantify the adsorption mechanism. For instance, Boi *et al.* [28] adopted a bi-Langmuir equation assuming that one solute can bind to more than one adsorption binding site.

The aim of the present paper was to study the viability of the separation of tripeptides in binary mixtures using a commercial flat-sheet ion-exchange membrane adsorber. The separation of biomolecules with similar molecular weights has not been much studied. However, several studies have focused on the recovery or removal of single biomolecule solutions. Triglycine (GGG), which is the simplest tripeptide, has been used as a model molecule to analyze the molecular interactions and physicochemical parameters of amino acids, peptides and even proteins. The adsorption of GGG involves the terminal amino or carboxyl groups. To study the role that the central amino acid in the tripeptide plays, the adsorption of glycine-histamine-glycine (GHG) and glycine-tyrosine-glycine (GTG) was analyzed for the first time here. First, we studied the adsorption of single peptide solutions using the Langmuir isotherm for equilibrium adsorption data, and the dynamic breakthrough curves were fitted to calculate the key parameters of the model for each tripeptide. The competitive adsorption between the tripeptides in binary solutions was evaluated using multicomponent isotherms based on the Langmuir equation. Finally, the separation of peptides was examined by dynamic adsorption.

2. Theory

2.1. Kinetic sorption process and isotherm equations

The kinetic sorption equations considered in this study were based on the well-known Langmuir isotherm, which was formulated by some assumptions: (i) each active adsorption site accepts only one molecule,

(ii) the adsorbed molecules are organized as a monolayer, and (iii) all adsorption sites are energetically equivalent. The time derivative of adsorbed concentration is defined by a second order kinetic reversible process between adsorption and desorption and assuming that there is no interaction between adsorbed molecules. The adsorption rate depends on the solute concentration in the liquid phase and the free adsorption sites, and the desorption rate depends only on the adsorbed concentration of solute:

$$\frac{\partial c_s}{\partial t} = k_a \cdot c \cdot \left(c_s^* - c_s\right) - k_d \cdot c_s \tag{1}$$

where c is the solute concentration in the liquid phase, c_s is the adsorbed solute concentration in the solid phase, c_s^* is the maximum adsorbed solute concentration in the solid phase and k_a and k_d are the adsorption and desorption rate constants, respectively. In steady state conditions, both sorption processes are equal, and the kinetic equation leads to the isotherm Langmuir equation:

$$c_{s\_eq} = \frac{b \cdot c_s^* \cdot c_{eq}}{1 + b \cdot c_s^* \cdot c_{eq}} \tag{2}$$

where c_{eq} is the equilibrium solute concentration in the liquid phase, c_{s_eq} is the equilibrium solute concentration in the solid phase, and b is the ratio between the adsorption and desorption rate constants of the single solute, $b = k_a/k_d$.

There have been several modifications of the Langmuir isotherm over the years, especially to describe competitive adsorption in a multicomponent mixture. The simplest equation reported is the non-modified Langmuir model, which considers that the desorption rate also depends on all solute adsorber concentrations. Therefore, the kinetic equation and the isotherm are written as follows:

$$\frac{\partial c_{si}}{\partial t} = k_{ai} \cdot c_i \cdot \left(c_{si}^* - c_{si}\right) - k_{di} \cdot \left(1 + \sum_{\substack{j=1 \\ j \neq i}}^{n} \left(\frac{k_{aj}}{k_{dj}} \cdot c_j\right)\right) \cdot c_{si} \tag{3}$$

$$c_{si\_eq} = \frac{b_i \cdot c_{si}^* \cdot c_{i\_eq}}{1 + \sum_{j=1}^{n} b_j \cdot c_{j\_eq}} \tag{4}$$

Notice that both equations depend on the individual adsorption/desorption rate constants (k_{ai} and k_{di}), and, unfortunately, they usually fail in the correlation of experimental competitive adsorption [32].

An improvement of the non-modified model is the extended Langmuir model, which assumes equal competition of all solutes for the same adsorption sites, and also that they have the same maximum adsorption capacity. Then, the kinetic and isotherm equations of the extended Langmuir model are:

$$\frac{\partial c_{si}}{\partial t} = k_{Eai} \cdot c_i \cdot \left(c_{Es}^* - c_{si}\right) - k_{Edi} \cdot \left(1 + \sum_{\substack{j=1 \\ j \neq i}}^{n} \left(\frac{k_{Eaj}}{k_{Edj}} \cdot c_j\right)\right) \cdot c_{si} \tag{5}$$

$$c_{si\_eq} = \frac{b_{Ei} \cdot c_{Es}^* \cdot c_{i\_eq}}{1 + \sum_{j=1}^{n} b_{Ej} \cdot c_{j\_eq}} \tag{6}$$

where c_{Es}^* is the maximum global adsorbed solute concentration in the solid phase and k_{Eai} and k_{Edi} are the adsorption and desorption rate constants, respectively. These three parameters can be determined from the competitive experimental data.

To achieve better accuracy for competitive adsorption, the non-modified Langmuir model may include a new parameter that quantifies the interaction between molecules, η_i, which is characteristic of each solute and depends on the concentrations of the other components in the mixture. The kinetic and isotherm equation of the modified Langmuir model are written as follows:

$$\frac{\partial c_{si}}{\partial t} = k_{ai} \cdot \frac{c_i}{\eta_i} \cdot \left(c_{si}^* - c_{si}\right) - k_{di} \cdot \left(1 + \sum_{\substack{j=1 \\ j \neq i}}^{n} \left(\frac{k_{aj}}{k_{dj}} \cdot \frac{c_j}{\eta_j}\right)\right) \cdot c_{si} \tag{7}$$

$$c_{si\_eq} = \frac{b_i \cdot c_{si}^* \cdot \frac{c_{i\_eq}}{\eta_i}}{1 + \sum_{j=1}^{n} b_j \cdot \frac{c_{j\_eq}}{\eta_i}} \tag{8}$$

where c_{si}^*, k_{ai} and k_{di} correspond to the single maximum adsorbed solute i concentration in the solid phase and adsorption and desorption rate constants, respectively.

More sophisticated models can be found in the literature, although we only considered the models based on the Langmuir isotherm. The parameters of the three isotherms were determined from the experimental data measured in steady state conditions.

2.2. Dynamic adsorption process

The differential mass balance of a reference solute in the ion exchange membrane adsorber contains the following terms: (1) the temporal variation of the solute concentration in the liquid phase, c_i, (2) the convection due to the axial liquid velocity, v, at the z coordinate, (3) the axial dispersion, D_{Li}, and 4) the source term due to the adsorption. Therefore, the mass balance over a section of the membrane for a multicomponent solution gives the following continuity equation [33]:

$$\varepsilon \cdot \frac{\partial c_i}{\partial t} + \varepsilon \cdot v \cdot \frac{\partial c_i}{\partial z} = \varepsilon \cdot D_{Li} \cdot \frac{\partial^2 c_i}{\partial z^2} - (1 - \varepsilon) \cdot \frac{\partial c_{si}}{\partial t} \tag{9}$$

The mass balance equation is solved using a conventional numerical solution method (Computational Fluid Dynamics, CFD) with the usual initial and boundary conditions:

$$c_i = 0 \quad at \quad z \geq 0, \ t = 0 \tag{10}$$

$$c_{si} = 0 \quad at \quad z \geq 0, \ t = 0 \tag{11}$$

Dirichlet boundary condition at $z = 0$:

$$c_i = c_{oi} \quad at \quad z = 0, \quad t > 0 \tag{12}$$

Neumann boundary condition at the outlet, where L is the membrane thickness:

$$\frac{\partial c_i}{\partial z} = 0 \quad at \quad z = L, \ t > 0 \tag{13}$$

The differential of adsorbed solute concentration versus time ($\partial c_{si}/\partial t$) is defined by the kinetic sorption equation, which quantifies the competitive adsorption between all solutes in the mixture. These equations were discussed in the previous section.

A more general and compact mathematical expression can be obtained by defining dimensionless parameters, which are independent of the feed and equilibrium adsorbed concentrations. The differential mass and initial and boundary conditions balance are rewritten as follows [34,35]:

$$\frac{\partial C_i}{\partial \tau} + \frac{\partial C_i}{\partial \zeta} = \frac{1}{Pe_i} \cdot \frac{\partial^2 C_i}{\partial \zeta^2} - m_i \cdot \frac{\partial C_{si}}{\partial \tau} \tag{14}$$

$$C_i = 0 \quad at \quad \zeta \geq 0, \ \tau = 0 \tag{15}$$

$$C_{si} = 0 \quad at \quad \zeta \geq 0, \ \tau = 0 \tag{16}$$

$$C_i = C_{oi} \quad at \quad \zeta = 0, \ \tau > 0 \tag{17}$$

$$\frac{\partial C_i}{\partial \zeta} = 0 \quad at \quad \zeta = 1,\ \tau > 0 \tag{18}$$

where C_i is the ratio between the punctual and the feed solute concentration in the liquid -phase, $C_i = c_i/c_{oi}$, C_{si} is the ratio between the punctual and the equilibrium feed solute concentration in the solid phase in equilibrium with c_{oi}, $C_{si} = c_{si}/c_{si\_eq\_o}$, ζ is a dimensionnless coordinate along the membrane, and $\zeta = z/L$, τ is a dimensionless time defined as the ratio between the current time and the characteristic time of the process, $\tau = t/t_{process}$, which is the average time taken by a liquid element to pass through the membrane, $t_{process} = L/v$. The axial Péclet number, Pe_i, is defined as the ratio of axial advection to axial diffusion as follows: $Pe_i = v \bullet L/D_{Li}$. The parameter m_i depends on the isotherm at point c_{oi}: $m_i = (1-\varepsilon)/\varepsilon \bullet c_{si\_eq\_o}/c_{oi}$.

The main advantage of using the dimensionless equation is that the kinetic and equilibrium sorption equations are independent of the competitive sorption model. Then, the kinetic sorption equation can also be written in dimensionless form as:

$$\frac{\partial C_{si}}{\partial \tau} = K_{ads,i} \cdot \left(C_i + \frac{1}{r_i} \cdot \left(1 + \sum_{\substack{j=1 \\ j \neq i}}^{n} r_j \cdot C_j \right) \right) \cdot \left(C_{si\_eq} - C_{si} \right) \tag{19}$$

At steady state, the adsorbed solute concentration is constant at all points on the membrane adsorber. Thus, the isotherm equation can also be written in a general form as:

$$C_{si\_eq} = \frac{r_i \cdot C_{i\_eq} \bullet C^*_{si}}{1 + \sum_{j=1}^{n} r_j \cdot C_{j\_eq}} \tag{20}$$

The parameters $K_{ads.i}$, r_i and C^*_{si} are detailed in Table 1, and their calculation depends on the kinetic process considered.

In the literature, the dynamic adsorption was analyzed mainly for single solute solutions and few publications have studied the adsorption of multi-solute solutions in membrane adsorbers [35,36]. Moreover, these attempts to fit binary-solute dynamic adsorption were conducted by the single-solute adsorption isotherms, and the breakthrough curves were not fitted satisfactorily. Therefore, the model proposed in the present study, with dimensionless parameters, is general and valid for competitive Langmuir isotherms, and the fitting parameter values can be compared directly.

Table 1
Parameters of the dimensionless model for each kinetic process.

Individual Langmuir kinetic process
$K_{ads} = \frac{L}{v} \bullet k_a \bullet c_o$ (–)
$r = b \bullet c_o$ (–)
$C^*_s = \frac{c^*_s}{c_{s\_eq\_o}}$ (–)
$c_{s\_eq\_o} = \frac{r \cdot c^*_s}{1+r}$ (mol L^{-1})
Extended Langmuir kinetic process
$K_{ads,i} = \frac{L}{v} \bullet k_{ai} \bullet c_{oi}$ (–)
$r_i = b_{Ei} \bullet c_{oi}$ (–)
$C^*_{si} = \frac{c^*_{Es}}{c_{si\_eq\_o}}$ (–)
$c_{si\_eq\_o} = \frac{r_i \cdot c^*_{Es}}{1 + \sum_{j=1}^{n} r_j}$ (mol L^{-1})
Modified Langmuir kinetic process
$K_{ads,i} = \frac{L}{v} \bullet k_{ai} \bullet \frac{c_{oi}}{\eta_i}$ (–)
$r_i = b_i \bullet \frac{c_{oi}}{\eta_i}$ (–)
$C^*_{si} = \frac{c^*_{si}}{c_{si\_eq\_o}}$ (–)
$c_{si\_eq\_o} = \frac{r_i \cdot c^*_{si}}{1 + \sum_{j=1}^{n} r_j}$ (mol L^{-1})

The model is governed by Eqs. (14)–(20), which were solved using the software "Mathematica" (Wolfram Research). The model depends on five independent dimensionless parameters for each solute, which can be estimated from different experiments. The equilibrium experiment permits the calculation of kinetic sorption parameters from the corresponding isotherm. These parameters allow the determination of the following dimensionless parameters: r_i, C^*_{si} and m_i. From the dynamic experiments, the dimensionless parameters Pe_i and $K_{ads,i}$ can be determined by matching the experimental and calculated breakthrough curves.

3. Experimental

3.1. Reagents and solutions

The molecules used in this study were three peptides, supplied by Sigma-Aldrich (Schnelldorf, Germany): glycine-glycine-glycine (GGG), glycine-histidine-glycine (GHG) and glycine-tyrosine-glycine (GTG). The three peptides have the same terminal amino acid group, but differ in their central amino acid. The main physical characteristics of these peptides are shown in Table 2. The isoelectric point was calculated from a mass balance and the acid dissociation constants. The three peptides show an isoelectric point between pH 6 and 8, which means that peptide precipitation is prevented. The rest of the chemicals used (HCl, KCl, $Na_2B_4O_7$ and NaOH) were supplied by Panreac (Barcelona, Spain).

The feed solutions were prepared by solubilizing the powder peptide in water at a global concentration of 1 mM and pH 4, which was fixed using HCl. At this pH, all peptides have a positive charge (Fig. 1), which means that peptide precipitation is prevented. The peptide molecule charge is calculated from the pKas. The presence of ion buffer significantly reduces the number of peptide molecules adsorbed and complicates the separation process due to the small size of the peptides [11]. All peptides were at least 95 % pure and the initial concentration reported in this study was that obtained after adjusting the concentration based on purity.

3.2. Experimental set-up

The adsorption experiments were conducted using the commercial membrane adsorber Sartobind S, which was supplied by Sartorius (Göttingen, Germany). The membrane cartridge is formed by three flat sheets of macroporous cross-linked cellulose and a hydrogel layer with sulfonic functional groups, creating a strong acid cation exchanger. The main features of the membrane adsorber are: a diameter of 25 mm (membrane area of 4.91 cm^2), an average membrane thickness of about 0.8 mm and a porosity of 78 % [38]. Solutions were placed in a plastic

Table 2
Properties of the studied peptides.

Characteristics	Peptide name		
	GGG	GHG	GTG
Molecular weight (g mol^{-1})	189.2	269.3	295.3
Number of amino groups	1	2	1
pK_{a1}[a]	3.23	3.08	3.10
pK_{a2}[a]	–	6.50	9.78
pK_{a3}[a]	8.09	9.50	8.06
pI[b]	5.66	8.0	5.58
Molecular diffusion coefficient[c] (m^2 s^{-1})	$5.71 \cdot 10^{-10}$	$5.33 \cdot 10^{-10}$	$5.18 \cdot 10^{-10}$

[a] pK_{a1} corresponds to terminal carboxylic group, pK_{a3} corresponds to terminal ammonium ion, and pK_{a2} corresponds to the ionizable group of the central amino acid.
[b] Isoelectric point was calculated from the pKas.
[c] The molecular diffusion coefficient of dyes was calculated using the Hayduk and Laudie method [37], where the LaBas molar volume was estimated using Cs Chem3D Ultra® (Molecular Modelling and Analysis).

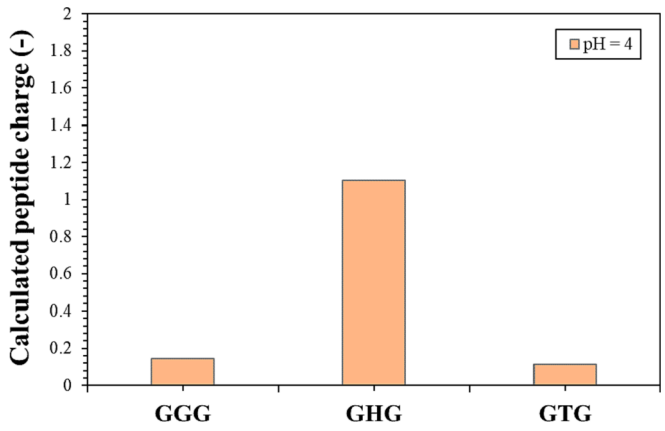

Fig. 1. Calculated peptide molecule charge for the three peptides at pH 4.

syringe and they were fed into the membrane cartridge via a single syringe pump NE-1000 (New Era Pump Systems Inc., Farmingdale, New York) set at flow rates of 1.0, 0.50 and 0.25 mL min^{-1}. The schematic representation of the experimental set up was shown in a previous publication [29]. Two experimental configurations were used in this study to analyze the adsorption peptides. First, isotherm experiments were conducted by pumping a fixed volume of the feed solution to the membrane cartridge in alternating cycles back and forth in a push–pull action with the syringe pump. After 48 h, equilibrium was reached in all cases. Second, dynamic experiments were performed by continuously pumping the feed solution in one direction to attain the breakthrough curves.

After an adsorption experiment, the membrane carbridge was washed with 20 mL of 0.1 M HCl to remove unbound peptides and the adsorbed molecules were eluted using a solution of 2 M KCl, until effluent was free of peptides. The membrane regeneration step was performed using 0.1 M HCl followed by ultra pure water, until neutral pH was obtained. Finally, the membrane was equilibrated before the next adsorption step, using 100 mL of 10^{-4} M HCl to fix the same pH of the feed solutions. Washing, desorption, regeneration and equilibration steps were conducted at 1 mL min^{-1}.

3.3. Capillary electrophoresis conditions

The peptide concentrations were analyzed using capillary electrophoresis equipment, which was supplied by Agilent Technologies (Waldbronn, Germany). This equipment has an on-column diode-array spectrophotometric detector. The capillary cartridge was formed from fused-silica capillaries (Polymicro Technologies, Phoenix, AZ, USA) with the following characteristics: length 48 cm, internal diameter 75 μm and external diameter 375 μm. The activation of new capillaries was conducted by flushing a solution of 1 M NaOH for 20 min and water for 30 min.

Injection of the samples into the capillary was carried out hydrodynamically at a pressure of 35 mbar for 5 s, and the voltage used for the electrophoretic separation was 25 kV in positive polarity for 5 min. The capillary temperature was kept constant at 25 °C and the buffer used to maintain the electrophoretic separation at a constant pH was 50 mM sodium tetraborate (pH 9).

Peptide detection was carried out at a wavelength of 195 nm through a UV window spaced at 48.5 cm from the capillary inlet [39]. As a result of this procedure, the electrophoretic signals of each peptide were separated, and the integration of peaks was accurate for the binary solutions.

The peptide concentration was calculated using calibration curves with standard solutions that were also measured at 195 nm. All these solutions were filtered through a 0.45 μm Nylon membrane before being introduced into the EC, to eliminate any possible solid that could block the capillary. Each electrophoretic measurement reported is the average of three replicates.

Before each run, the capillary was successively rinsed with 0.1 M NaOH for 5 min, with water for 5 min and finally with 50 mM sodium tetraborate for 5 min.

4. Results and discussion

4.1. Peptide adsorption isotherms in single solutions

The equilibrium adsorption isotherms of the three single peptide solutions are shown in Fig. 2. The adsorption affinities were very similar for GGG and GHG, although the peptide charges differed, being +0.15 for GGG and +1.1 for GHG. However, the adsorption concentration of GTG was high at all peptide concentrations in the liquid phase. For instance, the experimental adsorption concentrations were 0.180, 0.201 and 0.284 mol L^{-1} for GGG, GHG and GTG, respectively, for 1 mmol/L single peptide concentration in the final solution. Therefore, the differences observed in peptide isotherms are mainly due to the chemical characteristics of the central amino acid, rather than the peptide charge. A non-electrical interaction between the tyrosine amino acid present in GTG and the membrane matrix could be the reason for the higher adsorption of GTG.

The most common way to determine the Langmuir isotherm parameters of Eq (2) is linear regression following linearization of the isotherm equation, which can be done in four different ways [40,41]. The values of these parameters usually depend on the linear transformation used and they are significantly affected by the experimental error of adsorbed concentrations, especially at low or high concentrations [40]. More recently, some studies showed more precise and accurate parameter calculations using nonlinear rather than linear regression [41], mainly due to the use of the reciprocal concentration in linear transformations, which amplifies small deviations and thus yields worse results.

In this study, the estimation of Langmuir isotherm parameters c_s^* and b in single solutions was performed using the linearized equation proposed by Lineweaver–Burk, which is obtained by a direct reciprocal of the isotherm, and nonlinear regression, which was performed using the "NonlinearModelFit" function of Wolfram Mathematica. Table 3 shows the calculated parameters c_s^* and b, and the correlation coefficient, for both linear and non-linear correlation. Notice that similar calculated parameters were obtained for both methodologies. Nevertheless, the non-linear regression produced a better correlation coefficient. As shown in Fig. 2, the good fit of the experimental points to the Langmuir isotherm means that it is reasonable to assume monolayer adsorption. Given that the isotherm parameters of the binary solutions were to be

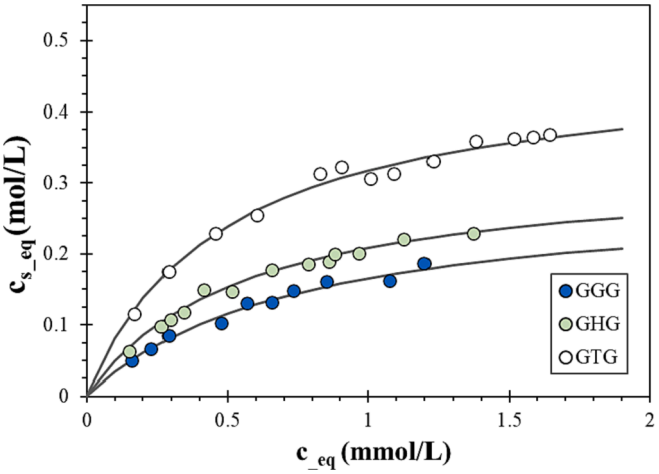

Fig. 2. Equilibrium adsorption isotherms of single peptide solutions at pH 4.

Table 3
Langmuir isotherm parameters for the three single peptide solutions calculated by the linear and non-linear regressions.

	b (L mol^{-1})	c_s^*(mol L^{-1})	R^2
Linear regression			
GGG	1297	0.303	0.9864
GHG	1790	0.327	0.9888
GTG	1885	0.484	0.9915
Non-linear regression			
GGG	1323	0.305	0.9911
GHG	1653	0.332	0.9943
GTG	2068	0.470	0.9961

calculated using non-linear regression, we used the values obtained with the non-linear regression for the single peptide Langmuir isotherm.

4.2. Peptide adsorption isotherms in binary solutions

The competitive adsorption between two peptides was studied in binary solutions containing GGG/GHG and GGG/GTG mixtures. The total peptide concentration in the liquid phase was fixed to 1 mM. GHG and GTG concentrations were varied to obtain different peptide concentration ratios. Fig. 3 shows the experimental adsorption values as a function of GGG molar fraction in the liquid phase for the two mixtures. It can be seen that the equilibrium adsorption concentrations of GGG in both mixtures were lower than the equilibrium adsorption concentrations of GHG and GTG, which indicates an interaction between the peptide molecules inside the membrane adsorber. In the literature, this reduction of adsorption affinities in binary solutions is attributed to the inhibition of adsorption between the solutes [42].

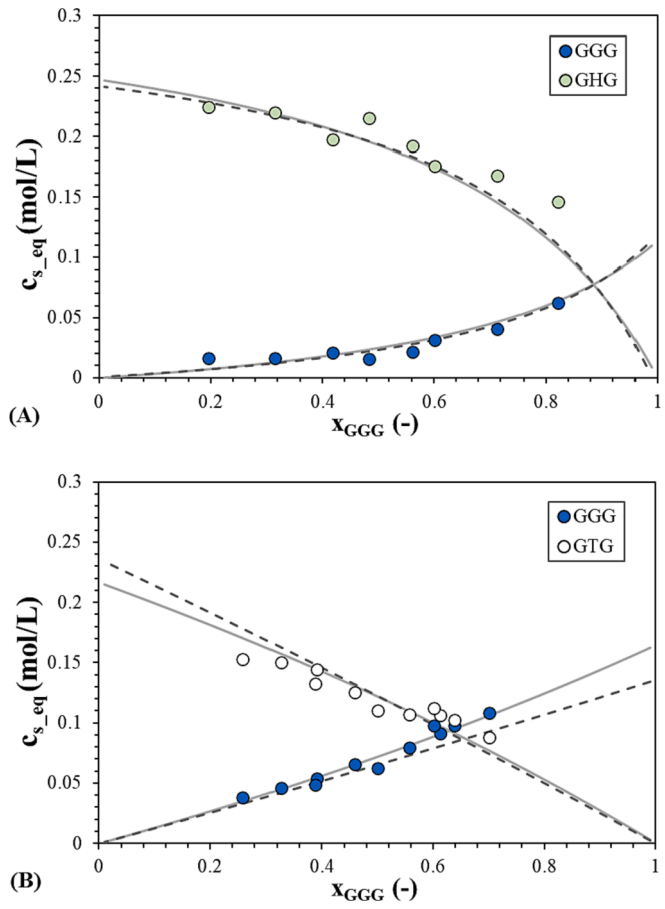

Fig. 3. Adsorbed peptide concentrations as a function of GGG peptide mass fraction in the liquid phase for the two binary solutions: (A) GGG/GHG mixtures and (B) GGG/GTG mixtures. Continuous lines correspond to calculated values with the extended Langmuir isotherm and discontinuous lines correspond to the modified Langmuir isotherm.

The experimental adsorbed concentration of both mixtures was fitted to multicomponent Langmuir isotherms, which were described in section 2.1, to find the most appropriate competitive isotherm for the binary adsorption of GGG/GHG and GGG/GTG. The non-modified Langmuir isotherm, which assumes that the single adsorption parameters are applicable to binary solutions, was not able to fit the experimental data. However, good fits were found with the extended and modified Langmuir isotherms, as shown in Fig. 3. It can be seen that the adsorbed concentration calculated with the two competitive isotherms correlated well with the experimental data for the two mixtures. The parameters of the two isotherms were estimated by a non-linear regression using the "NonlinearModelFit" function of Wolfram Mathematica, and Table 4 shows the estimated values and the non-linear correlation coefficient. For GGG/GHG solutions, the extended Langmuir isotherm fitted the competitive adsorption reasonably well with a non-linear correlation coefficient of around 0.978 for the two peptides. Nevertheless, the values of the ratio between the adsorption and desorption rate constants, b_E, differed significantly from parameter b of the single solution, leading to a significant increase for GHG, from 1653 L mol^{-1} to 4715 L mol^{-1}. This means that the presence of GGG increased the adsorption rate constant of GHG by 3-fold, which is not plausible in a competitive adsorption process. The modified Langmuir isotherm also showed a good fit to the experimental data with a non-linear correlation coefficient of around 0.98 for the two peptides. The values of the interaction parameter, η, were higher than unity for GHG and lower than unity for GGG, as can be expected for competitive adsorption [43].

In contrast, the extended Langmuir isotherm showed a better fit to the experimental data for GGG/GTG mixtures than the modified isotherm, with a non-linear correlation coefficient higher than 0.99. The calculated b_E values were lower than the b values of the single solutions due to competitive adsorption. The extended isotherm assumes equal competition of all solutes for the same adsorption sites and the same maximum adsorption capacity that can be expected to be the sum of the capacities of the two solutes. Nevertheless, the maximum adsorbed concentration estimated with the extended isotherm for GGG/GTG mixtures was 0.401 mol/L, which was considerably lower than the sum of the cs^* of GGG and GTG for single solutions. This observation is in line with the inhibited adsorption mentioned above, which indicates non-uniform adsorption competition for the binding sites of the adsorbent [44]. The modified Langmuir isotherm did not improve the fit of binary adsorption of GGG/GTG mixtures (non-linear correlation coefficient lower than 0.99), with the interaction parameters being higher than 1 for both solutes.

In summary, the modified Langmuir isotherm showed a better correlation with the equilibrium adsorption concentrations of GGG/GHG solutions, and the extended Langmuir isotherm correlated better with the GGG/GTG solutions.

Table 4
Parameters of the competitive Langmuir isotherms for the two binary peptide solutions.

	Extended Langmuir isotherm			Modified Langmuir isotherm	
	b_E (L mol^{-1})	c_{Es}^*(mol L^{-1})	R^2_{nl}	ηi	R^2_{nl}
Mixture 1					
GGG	503	0.309	0.9789	2.69	0.9803
GHG	4715	0.309	0.9772	0.31	0.9794
Mixture 2					
GGG	702	0.401	0.9962	1.51	0.9896
GTG	1153	0.401	0.9953	2.09	0.9891

4.3. Dynamic adsorption experiments of single solutes

Dynamic adsorption was studied by continuously pumping the solution and, as a result, the breakthrough curve was obtained at the exit of the membrane adsorber when it was saturated. After determining the isotherm parameters, which allows the calculation of r, p and m, the breakthrough curve depends only on Pe and K_{ads}. The axial dispersion coefficient was determined experimentally by decoupling yields both fitting parameters under non-adsorbing conditions, which were obtained by conducting the experiments with a strongly acid cation exchange membrane adsorber with sulfonic groups (Sartobind S). Assuming that peptide molecules cannot electrostatically interact with the diethylamine groups of the membrane, breakthrough curves were calculated using different Pe values (Fig. 4). The experimental breakthrough curve did not fit well with the molecular diffusion coefficient and the effect of axial dispersion should be considered, since the Sartobind membranes have anisotropic micropores [45]. None of the calculated breakthrough curves represent the experimental data with a Pe number ranging from 10 to 1. Therefore, fitting the experimental breakthrough curve requires considering some non-electrostatic adsorption or absorption mechanisms and the axial dispersion. Consequently, the dispersion and adsorption mechanism cannot be decoupled from the cationic membrane adsorber.

Fig. 5 shows the breakthrough curves in adsorbing conditions (Sartobind S) for the three single peptides at three flow rates (1.0, 0.50 and 0.25 mL min^{-1}) and at a fixed solute feed concentration of 1 mM. The three breakthrough curves are located at different dimensionless times, thereby denoting the different adsorption capabilities of the peptides to the membrane adsorber. For instance, membrane saturation, which is obtained when the outlet dimensionless concentration is equal to 1, was observed at the dimensionless time of 152, 179, and 228 for GGG, GHG and GTG, respectively, at 1 mL min^{-1}. A similar pattern was observed for the other two flow rates. The breakthrough point, which is the time taken to reach 5 % of the saturation concentration, showed the same pattern. The breakthrough points for GGG and GHG were very similar, being 34.1 and 39.8, respectively, at 0.50 mL min^{-1}, as is to be expected from the equilibrium data. The breakthrough point was displaced to 53.7 for GYG, due to its higher affinity to membrane adsorption sites.

Fig. 5 also shows the breakthrough curves fitted by the model for the three single peptide solutions and flow rates. The Pe and K_{ads} numbers were found by minimizing the least squares objective function between calculated and experimental data, and the r and m dimensionless parameters were calculated from the Langmuir isotherm parameters. In general, the calculated and experimental breakthrough curves were correlated with high agreement (Fig. 5). Only small deviations between them were observed, which might have been due to experimental error and/or membrane irregularities. The estimated Pe values depend on the peptide molecule, and also showed flow rate dependency. As expected from the equilibrium data, GTG showed the highest adsorption affinity, with a k_a constant value of 47.6 L mol^{-1} s^{-1}; GHG and GGG showed a more similar affinity, with a k_a constant value of 38.5 L mol^{-1} s^{-1} and 35.7 L mol^{-1} s^{-1}, respectively. Therefore, some non-electrostatic interactions between the tyrosine amino acid and the membrane matrix, or tyrosine with other GTG molecules, could be the result of this higher

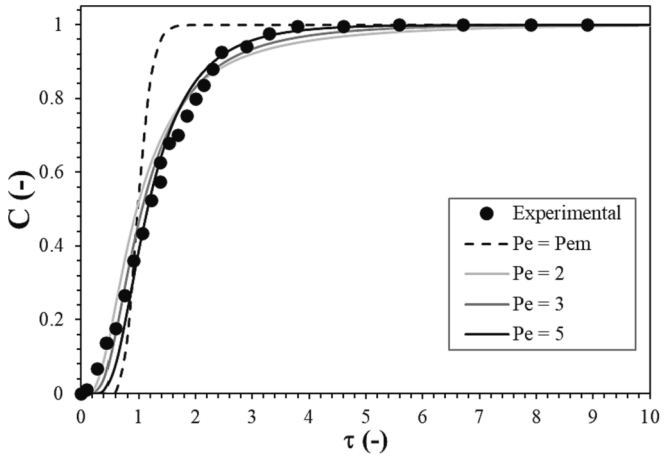

Fig. 4. Experimental breakthrough curve with non-adsorbing membrane adsorber when the flow rate was 1.0 mL min^{-1}. Solid lines correspond to simulations with different Pe values and low adsorption (m = 1 and K_{ads} =∞).

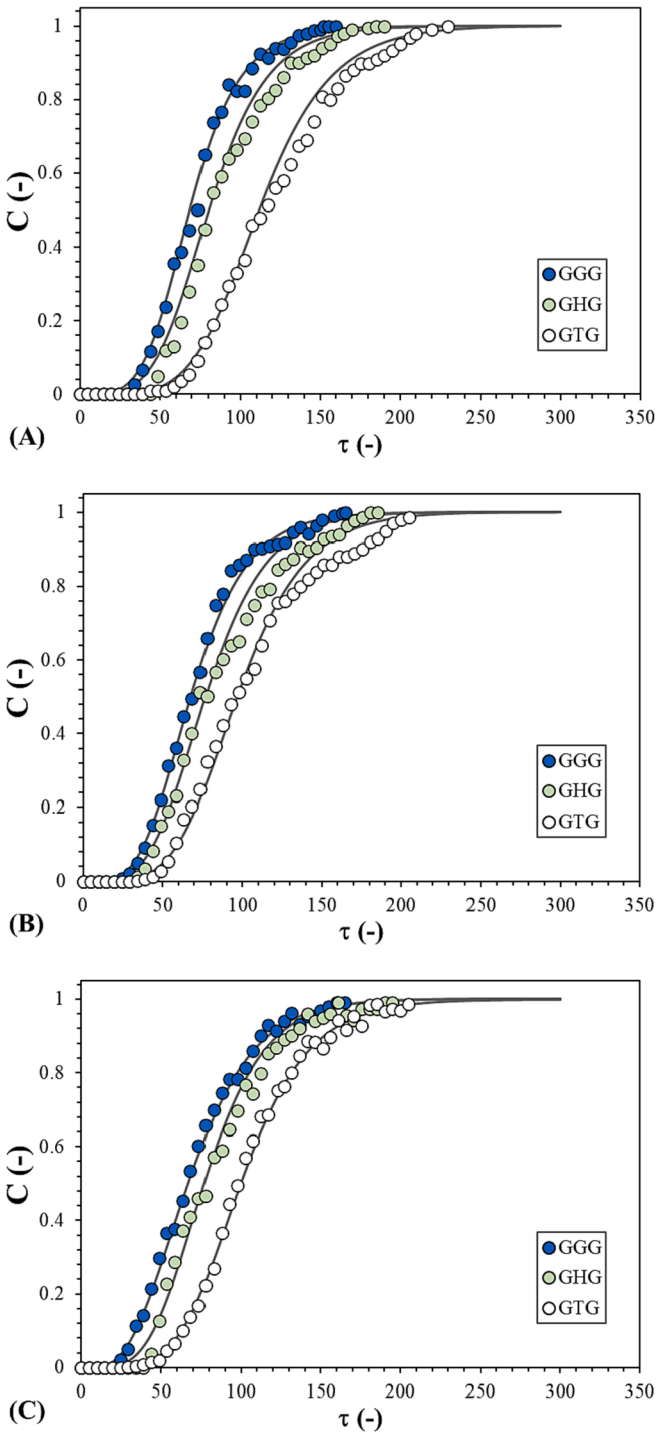

Fig. 5. Experimental and calculated breakthrough curves of three single peptide solutions at flow rates of (A) 1.0 mL min^{-1}, (B) 0.50 mL min^{-1}, and (C) 0.25 mL min^{-1}.

affinity of GTG than the other two peptides.

The axial dispersion coefficient, D_L, for the three peptides was calculated from *Pe* and their values are shown in Fig. 6. The D_L increases with the feed flow rateand the values are one order of magnitude higher than the molecular diffusion coefficient, which means that the axial dispersion component is significant in the membrane adsorber [46]. As the D_L values for the three peptides were very similar at a fixed flow rate, the mean value was calculated and a linear increase with feed flow rate was obtained (Fig. 6), as previously reported elsewhere [47].

Table 5 shows the breakthrough time (t_b), breakthrough adsorption capacity (c_{sb}) and saturation time (t_s) and saturated adsorption capacity (c_{ss}) for the three single peptides as a function of flow rate. The four parameters were estimated from the fitting breakthrough curves. The breakthrough time and breakthrough adsorption capacity decreased with the flow rate for the three peptides. Nevertheless, saturation time and saturated adsorption capacity were also independent of flow rate and the saturated capacity corresponded well with the adsorption equilibrium showed in Fig. 2.

4.4. Dynamic adsorption of binary mixtures

The separation of peptides in binary solutions (GGG/GHG and GGG/GTG) was also studied in two different mixtures of the solutions: 0.5 mM GGG/0.5 mM GHG or GTG and 0.75 mM GGG/0.25 mM GHG or GTG. Fig. 7 shows the experimental breakthrough curves for the four mixtures, which were obtained at 1.0 mL min^{-1}. A clear difference between the two binary solutions can be seen with the presence of a significant overshooting in GGG/GHG solutions. The GGG peptide, which is the smallest peptide, was fully adsorbed during the initial period and started to exit the membrane adsorber at a dimensionless breakthrough time of about 22. After this time, the GHG peptide displaced the adsorbed GGG molecules and the dimensionless GGG concentration at the exit increased to higher values of 1. The GHG peptide showed a dimensionless breakthrough time of about 80 and the dimensionless saturation time for both peptides was above 500, when the dimensionless concentrations were 1. A similar trend was observed for the 0.75 mM GGG/0.25 mM GHG mixture. The higher feed concentration of GGG reduced the ability of GHG molecules to desorb the adsorbed GGG molecules and the overshooting reached a lower dimensionless concentration. As a result, the dimensionless breakthrough and saturation times of GHG moved to 120 and 600, respectively.

The breakthrough curves of the GGG/GTG solutions showed some differences (Fig. 7). The breakthrough curves of the GGG peptide show less overshooting, being nonexistent for the 0.75 mM GGG/0.25 mM GTG mixture. As shown in Fig. 7, the GGG peptide left the membrane adsorber faster than the GTG peptide, and the dimensionless breakthrough time was about 30 for GGG and 59 for GTG for the 0.5 mM GGG/0.5 mM GTG mixture. These relatively similar values mean that both peptides remain inside the membrane adsorber at almost the same concentration at which they entered. Therefore, the separation of GGG and GTG peptides in these conditions is very difficult. These results indicate the preference of the membrane to adsorb the three compounds in the following sequence: GHG > GTG > GGG.

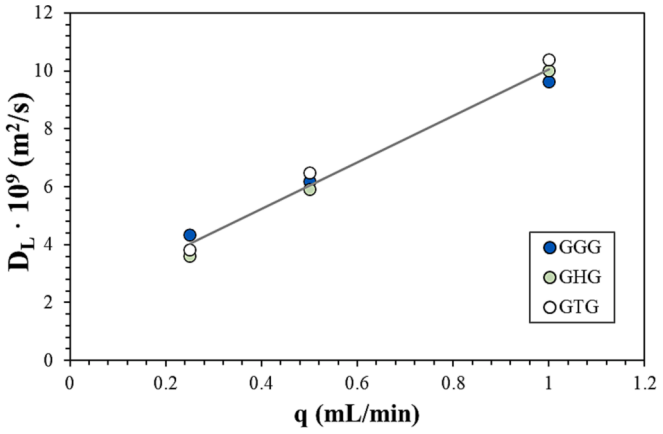

Fig. 6. Calculated axial dispersion coefficients as a function of flow rates.

Table 5
Breakthrough time (t_b), breakthrough adsorption capacity (c_{sb}) and saturation time (t_s) and saturated adsorption capacity (c_{ss}) for the three peptides in single solutions as a function of flow rate. Parameters were calculated from the fitting curves.

Peptide	q (mL min^{-1})	t_b(min)	c_{sb}(mol L^{-1})	t_s(min)	c_{ss}(mol L^{-1})
GGG	1	14.1	0.0816	123	0.174
	0.5	13.1	0.0758	123	0.173
	0.2	11.2	0.0653	123	0.174
GHG	1	16.2	0.0941	123	0.188
	0.5	15.8	0.0913	123	0.186
	0.2	15.9	0.0922	123	0.185
GTG	1	25.1	0.146	123	0.280
	0.5	20.7	0.120	123	0.262
	0.2	20.2	0.119	123	0.247

Fig. 7 shows also the fitted breakthrough curves, which were obtained using the model dimensionless parameters (*Pe* number and k_a constant) obtained in the calculations of the breakthrough curves of single peptide solutions. After obtaining the equilibrium data, the *r* and *m* parameters of GGG/GHG solutions were calculated using the modified Langmuir isotherm and the data for GGG/GTG mixtures were calculated using the extended Langmuir isotherm (Table 4). Satisfactory correlation was obtained for all mixtures and the main differences were found in the degree of overshooting with a dimensionless GGG concentration higher than 1, especially for GGG/GHG solutions. This could be due to the small change in solution pH during the adsorption process or the presence of some interaction between the two peptides [48,49].

Based on the fitting curves, the calculations of breakthrough time and adsorption capacity and saturation time and saturated adsorption capacity are shown in Table 6. In the GGG/GHG solutions, the breakthrough time of GGG and GHG was shortened and extended, respectively, and both breakthrough and saturated adsorption capacity were decreased significantly for GGG and increased for GHG, as expected from the binary equilibrium isotherm. In particular, the saturated adsorption capacity of GGG in 0.5 mM GGG/0.5 mM GHG mixture fell by around 97 %, which evidenced the higher adsorption affinity of GHG. In the GGG/GTG solutions, the calculated values are more similar to the single solution values (Table 6), and the competitive adsorption between GGG and GTG is much lower than between GGG and GHG. Following the binary isotherm, the saturated adsorption capacity of GGG is higher than the GTG in the 0.75 mM GGG/0.25 mM GTG mixture. With respect to axial dispersion, some interaction between adsorption/desorption processes and axial dispersion is noted, since D_L is reduced for the three peptides in the mixtures. For instance, the decrease in D_L for GGG was 25 %, compared with 18 % for both GHG and GTG.

Having found the model's parameters, dynamic adsorption inside the membrane can be analyzed at any position and time. For instance, Fig. 8 shows the calculated dimensionless adsorption concentrations of both peptides inside the membrane adsorber at different dimensionless times for the 0.5 mM GGG/0.5 mM GHG mixture and the 0.5 mM GGG/0.5 mM GTG mixture. Very different profiles are apparent for the two mixtures. The dimensionless adsorption concentration for GGG in the 0.5 mM GGG/0.5 mM GHG mixture was higher than 1 and it increased significantly with time, displacing the maximum values to the exit from the membrane. The dimensionless adsorption concentration higher than 1 means that the GGG adsorbed concentration is higher than the adsorbed equilibrium value corresponding to the feed concentration. This means that GGG concentration in the liquid phase, in some places inside the membrane, is higher than the feed concentration because

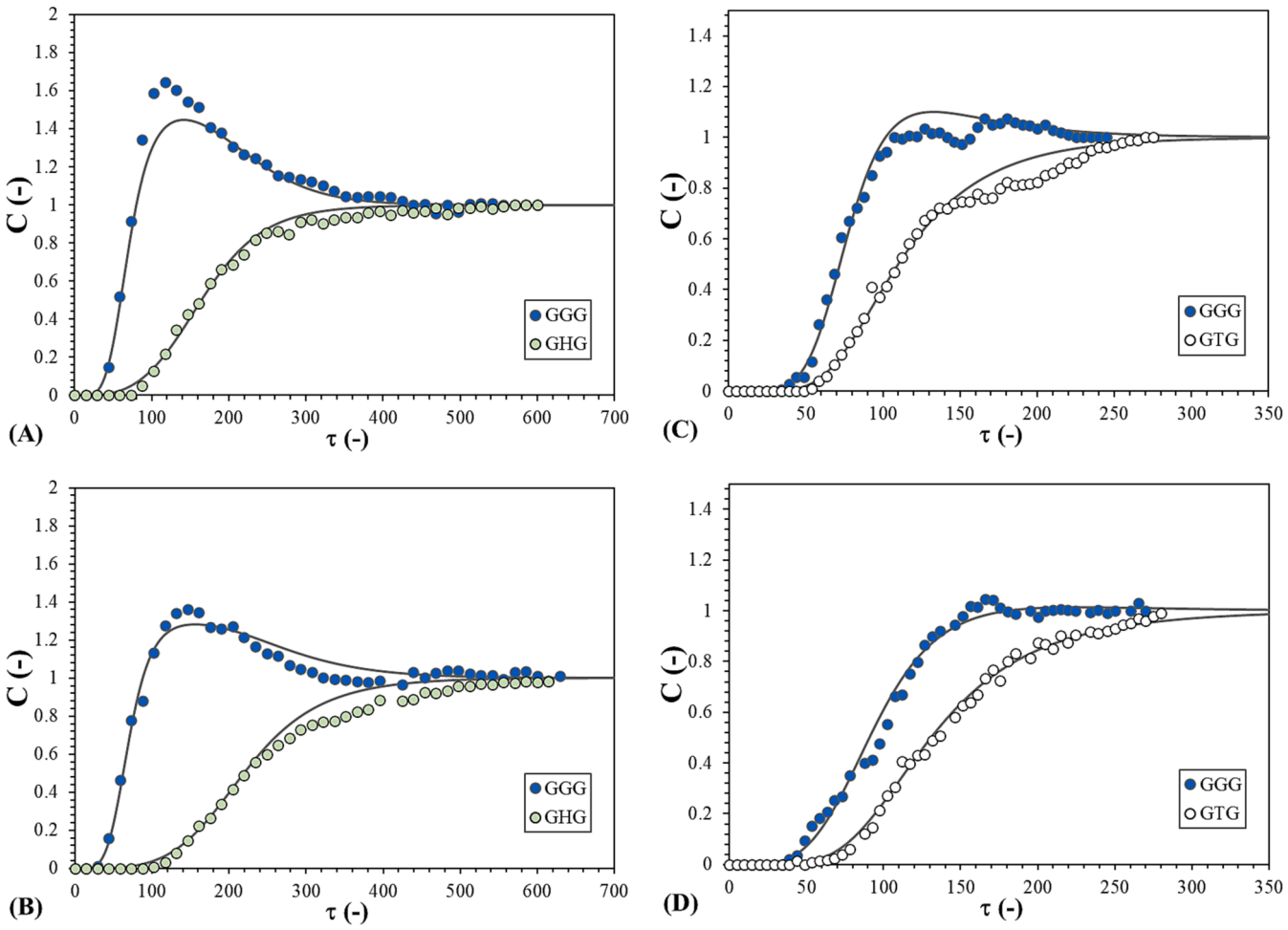

Fig. 7. Experimental and calculated breakthrough curves of binary peptide mixtures at 1 mL min^{-1}: (A) 0.5 mM GGG/0.5 mM GHG mixture, (B) 0.75 mM GGG/0.25 mM GTG mixture, (C) 0.5 mM GGG/0.5 mM GTG mixture, (D) 0.75 mM GGG/0.25 mM GTG mixture.

Table 6
Breakthrough time (t_b), breakthrough adsorption capacity (c_{sb}) and saturation time (t_s), saturated adsorption capacity (c_{ss}) and axial dispersion coefficient (D_L) for the four binary mixtures. Parameters were calculated from the fitting curves.

Peptide mixture	$D_L \cdot 10^9$ ($m^2\ s^{-1}$)	t_b (min)	c_{sb} (mol L^{-1})	t_s (min)	c_{ss} (mol L^{-1})
Mixture 1 (GGG/GHG)					
0.5 mM GGG	7.34	13.8	0.0402	246	0.00504
0.5 mM GHG	8.13	39.3	0.114	246	0.183
Mixture 2 (GGG/GHG)					
0.75 mM GGG	7.20	12.6	0.0516	246	0.0310
0.25 mM GHG	8.67	44.8	0.0729	246	0.140
Mixture 3 (GGG/GTG)					
0.5 mM GGG	7.25	15.8	0.0409	143	0.0589
0.5 mM GTG	8.50	24.5	0.0561	143	0.116
Mixture 4 (GGG/GTG)					
0.75 mM GGG	7.21	14.9	0.0450	143	0.105
0.25 mM GTG	8.43	28.0	0.0423	143	0.0732

GHG molecules replace a large amount of the previously adsorbed GGG molecules, increasing the GGG uptake concentration [50]. As observed in the equilibrium data, the two peptides showed highly competitive adsorption in GGG/GHG solutions. Nevertheless, the solute uptake concentrations for both peptides in the 0.5 mM GGG/0.5 mM GTG mixture showed a similar profile inside the membrane although the GGG uptake concentration was always higher than the GTG uptake concentration and achieved values higher than 1 only after longer times. Notice that the molecular charge of both peptides was the same (Fig. 1) and the differences in adsorption could be due to the stronger interaction of GTG peptide with the membrane adsorber via the hydroxyl group of the central tyrosine amino acid.

The molar fraction adsorbed to the solid phase, X_s, was also calculated using the following equation, which evaluates the total adsorbed quantity in the whole membrane at each dimensionless time:

$$X_s = \frac{\left| c_{s\_eq\_o} \bullet \int_0^L Cs \bullet d\zeta \bullet \right|_{GGG}}{\left| c_{s\_eq\_o} \bullet \int_0^L Cs \bullet d\zeta \right|_{GGG} + \left| c_{s\_eq\_o} \bullet \int_0^L Cs \bullet d\zeta \right|_{GHGorGTG}} \quad (21)$$

Fig. 9 shows the evolution of adsorbed molar fractions of GHG and GTG for the two mixtures: 0.5 mM GGG/0.5 mM GHG and 0.5 mM GGG/0.5 mM GTG. After short times, when the adsorption sites are free, the adsorbed molar fractions remained almost constant, were close to 50 % and both peptides had a similar adsorption affinity. After the breakthrough point, the adsorbed molar fractions progressively increased, especially for GHG in the 0.5 mM GGG/0.5 mM GHG mixture, showing the different degrees of adsorption affinity of the three peptides. Ultimately, the adsorbed molar fractions reached a constant value that corresponded to the equilibrium value of each mixture.

The separation of peptides in binary solutions was quantified by the calculation of cumulative solute concentration in the outlet stream at the breakthrough point for GHG or GTG, $c_{c,i}$, as follows:

$$c_{c,i} = \frac{1}{V_{b2}} \bullet \int_0^{V_{b2}} c_i \bullet dV \quad (22)$$

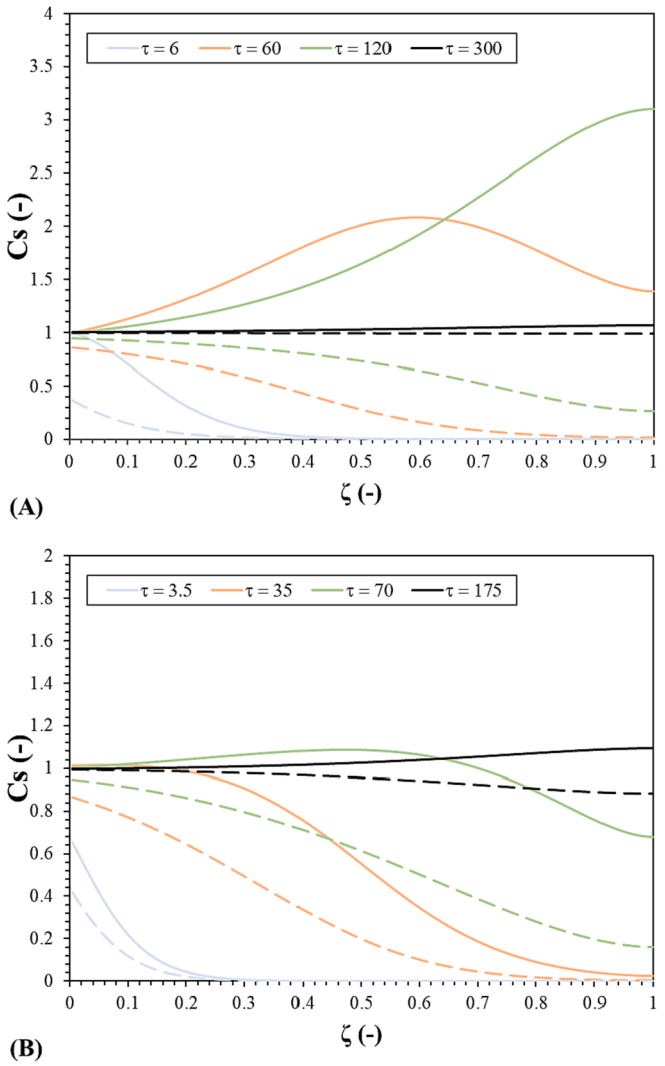

Fig. 8. Calculated dimensionless adsorption concentrations of both peptides inside the membrane adsorber at different dimensionless times for (A) 0.5 mM GGG/0.5 mM GHG mixture and (B) 0.5 mM GGG/0.5 mM GTG mixture. Continuous lines correspond to GGG and discontinuous lines correspond to GHG or GTG in the mixtures.

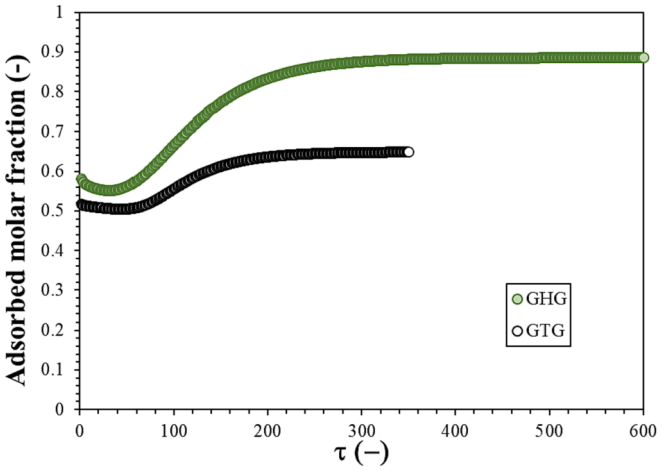

Fig. 9. Adsorbed molar fraction inside the membrane as a function of dimensionless time for GHG in the 0.5 mM GGG/0.5 mM GHG mixture and GTG in the 0.5 mM GGG/0.5 mM GTG mixture.

where V_{b2} is the volume in the outlet stream corresponding to the breakthrough point of the GHG or GTG, c_i is the punctual solute concentration in the outlet stream at each volume V, and i indicates the solute: $i = 1$ for GGG and $i = 2$ for GHG or GTG. The experimental values of the breakthrough curves up to V_{b2} were adjusted to a polynomial equation to determine more exactly the numerical integration in Eq. (22). Table 7 shows the cumulative solute concentrations calculated for the four mixtures. As expected, the molar GGG fraction was more than 0.9 for all mixtures, nevertheless the cumulative GGG concentrations in the outlet stream were only significant for GGG/GHG solutions. The GGG recovery was higher than 35 %, and was 55 % for the 0.75 mM GGG/0.25 mM GHG mixture.

5. Conclusions

The adsorption of tripeptides (GGG, GHG and GTG) on a commercial ion-exchange membrane adsorber was analyzed in equilibrium and dynamic experiments. The adsorption of single peptide solutions was analyzed using the continuity equation coupled with the Langmuir isotherm. GTG showed the highest adsorption affinity, followed by GHG and GGG. The breakthrough curves were fitted by fixing the adsorption kinetic rate constant for each peptide and depended on the axial dispersion coefficient, which was almost the same value for all three peptides, and showed a significant dependence on flow rate.

In binary peptide solutions, the equilibrium adsorption of GGG/GHG solutions showed a better fit to the modified Langmuir isotherm, indicating that GHG has the highest affinity to binding sites due to its having the highest molecular charge among the three peptides. The GGG/GTG solutions showed lower competitive adsorption and the extended Langmuir isotherm fitted the equilibrium data better. While the two peptides have a similar molecular charge, some non-electrostatic interactions between the tyrosine amino acid and the membrane matrix may be responsible for the different adsorption affinities of GGG and GTG. Thereby, the separation between GGG and GHG was achieved by dynamic experiments, during the initial period of time when GHG was fully adsorbed and pure GGG was eluted from the membrane adsorber. The GGG recovery was higher than 35 % and the GGG molar fraction in the outlet stream was higher than 0.994. In contrast, no significant separation was achieved between GGG and GTG.

CRediT authorship contribution statement

Jordi Labanda: Conceptualization, Investigation, Writing – original draft, Methodology, Formal analysis. **Joan Llorens:** Supervision, Project administration, Funding acquisition, Conceptualization, Writing – review & editing.

Declaration of Competing Interest

The authors declare that they have no known competing financial interests or personal relationships that could have appeared to influence the work reported in this paper.

Table 7
Calculated GGG concentrations between breakthrough times for the four mixtures.

Feed concentration ratio	Cumulative GGG concentration	Molar GGG fraction	GGG recovery
0.5 mM GGG/0.5 mM GHG	0.188 mM	0.9943	37.6 %
0.75 mM GGG/0.25 mM GHG	0.419 mM	0.9975	55.7 %
0.5 mM GGG/0.5 mM GTG	0.0192 mM	0.9062	3.84 %
0.75 mM GGG/0.25 mM GTG	0.0531 mM	0.9325	7.08 %

Data availability

Data will be made available on request.

Acknowledgements

The authors are grateful to the Spanish Ministerio de Ciencia e Innovacion (Project CTQ2009–11465) for funds received to carry out this study.

References

[1] M. Hajfathalian, S. Ghelichi, P.J. García-Moreno, A.-D. Moltke Sørensen, C. Jacobsen, P.J. Garc ıa-Moreno, Critical reviews in food science and nutrition peptides: production, bioactivity, functionality, and applications Peptides: Production, bioactivity, functionality, and applications (2017), 10.1080/10408398.2017.1352564.

[2] N. Abd-Talib, E. Liza, A. Yaji, N. Suraya, A. Wahab, N. Razali, K. Yong, T. Len, J. Roslan, N. Saari, K. Faizal, P'. Ee, Bioactive peptides and its alternative processes: a review, Biotechnol. Bioprocess. Eng. 27 (2022) 306–335, https://doi.org/10.1007/s12257-021-0160-8.

[3] W.H. Yu, N. Li, D.S. Tong, C.H. Zhou, C.X. Lin, C.Y. Xu, Adsorption of proteins and nucleic acids on clay minerals and their interactions: a review, Appl. Clay Sci. 80–81 (2013) 443–452, https://doi.org/10.1016/J.CLAY.2013.06.003.

[4] A. Kasprzhitskii, G. Lazorenko, D.S. Kharytonau, M.A. Osipenko, A.A. Kasach, I. I. Kurilo, Adsorption mechanism of aliphatic amino acids on kaolinite surfaces, Appl. Clay Sci. 226 (2022), 106566, https://doi.org/10.1016/J.CLAY.2022.106566.

[5] J. Ikhsan, B.B. Johnson, J.D. Wells, M.J. Angove, Adsorption of aspartic acid on kaolinite, J. Colloid Interface Sci. 273 (2004) 1–5, https://doi.org/10.1016/J.JCIS.2004.01.061.

[6] E. Titus, A.K. Kalkar, V.G. Gaikar, Equilibrium studies of adsorption of amino acids on NaZSM-5 zeolite, Colloids Surfaces A Physicochem. Eng. Asp. 223 (2003) 55–61, https://doi.org/10.1016/S0927-7757(03)00131-6.

[7] R. Wijntje, H. Bosch, A.B. de Haan, P.J.T. Bussmann, Influencing the selectivity of zeolite Y for triglycine adsorption, J. Chromatogr. A. 1142 (2007) 39–47, https://doi.org/10.1016/J.CHROMA.2006.10.056.

[8] L. Cermakova, I. Kopecka, M. Pivokonsky, L. Pivokonska, V. Janda, Removal of cyanobacterial amino acids in water treatment by activated carbon adsorption, Sep. Purif. Technol. 173 (2017) 330–338, https://doi.org/10.1016/J.SEPPUR.2016.09.043.

[9] I. Kopecka, M. Pivokonsky, L. Pivokonska, P. Hnatukova, J. Safarikova, Adsorption of peptides produced by cyanobacterium *Microcystis aeruginosa* onto granular activated carbon, Carbon N. Y. 69 (2014) 595–608, https://doi.org/10.1016/J.CARBON.2013.12.072.

[10] M. Liu, J. Huang, Y. Deng, Adsorption behaviors of l-arginine from aqueous solutions on a spherical cellulose adsorbent containing the sulfonic group, Bioresour. Technol. 98 (2007) 1144–1148, https://doi.org/10.1016/J.BIORTECH.2006.03.026.

[11] R. Wijntje, H. Bosch, A.B. De Haan, P. Bussmann, Adsorbent Selection by Functional Group Interaction Screening for Peptide Recovery, 2005.

[12] Z. Hu, Z. Chen, X. Chen, J. Wang, Advances in the adsorption/enrichment of proteins/peptides by metal–organic frameworks-affinity adsorbents, TrAC Trends Anal. Chem. 153 (2022), 116627, https://doi.org/10.1016/J.TRAC.2022.116627.

[13] M.A. Khan, A.A. Alqadami, S.M. Wabaidur, M.R. Siddiqui, B.H. Jeon, S. A. Alshareef, Z.A. Alothman, A.E. Hamedelniel, Oil industry waste based non-magnetic and magnetic hydrochar to sequester potentially toxic post-transition metal ions from water, J. Hazard. Mater. 400 (2020), 123247, https://doi.org/10.1016/J.JHAZMAT.2020.123247.

[14] S.M. Wabaidur, M.A. Khan, M.R. Siddiqui, M. Otero, B.H. Jeon, Z.A. Alothman, A. A.H. Hakami, Oxygenated functionalities enriched MWCNTs decorated with silica coated spinel ferrite – a nanocomposite for potentially rapid and efficient de-colorization of aquatic environment, J. Mol. Liq. 317 (2020), 113916, https://doi.org/10.1016/J.MOLLIQ.2020.113916.

[15] I. Ali, O.M.L. Alharbi, Z.A. ALOthman, A.M. Al-Mohaimeed, A. Alwarthan, Modeling of fenuron pesticide adsorption on CNTs for mechanistic insight and removal in water, Environ. Res. 170 (2019) 389–397, https://doi.org/10.1016/J.ENVRES.2018.12.066.

[16] K. Niedergall, M. Bach, T. Hirth, G.E.M. Tovar, T. Schiestel, Removal of micropollutants from water by nanocomposite membrane adsorbers, Sep. Purif. Technol. 131 (2014) 60–68, https://doi.org/10.1016/J.SEPPUR.2014.04.032.

[17] R. Ghosh, Protein separation using membrane chromatography: opportunities and challenges, J. Chromatogr. A. 952 (2002) 13–27, https://doi.org/10.1016/S0021-9673(02)00057-2.

[18] C. Boi, Membrane adsorbers as purification tools for monoclonal antibody purification, J. Chromatogr. B. 848 (2007) 19–27, https://doi.org/10.1016/J.JCHROMB.2006.08.044.

[19] E. Klein, Affinity membranes: a 10-year review, J. Memb. Sci. 179 (2000) 1–27, https://doi.org/10.1016/S0376-7388(00)00514-7.

[20] C. Boi, A. Malavasi, R.G. Carbonell, G. Gilleskie, A direct comparison between membrane adsorber and packed column chromatography performance, J. Chromatogr. A. 1612 (2020), 460629, https://doi.org/10.1016/J.CHROMA.2019.460629.

[21] F. Hagemann, D. Wypysek, K. Baitalow, P. Adametz, V. Thom, M. Wessling, Why device design is crucial for membrane adsorbers, J. Chromatogr. Open. 2 (2022), 100029, https://doi.org/10.1016/J.JCOA.2021.100029.

[22] M.O. Herigstad, S. Dimartino, C. Boi, G.C. Sarti, Experimental characterization of the transport phenomena, adsorption, and elution in a protein A affinity monolithic medium, J. Chromatogr. A. 1407 (2015) 130–138, https://doi.org/10.1016/J.CHROMA.2015.06.045.

[23] L. Raiado-Pereira, A.P. Carapeto, A.M. Botelho Do Rego, M. Mateus, Grafting hydrophobic and affinity interaction ligands on membrane adsorbers: a close-up "view" by X-ray photoelectron spectroscopy, Sep. Purif. Technol. 93 (2012) 75–82, https://doi.org/10.1016/J.SEPPUR.2012.03.028.

[24] H. Trnovec, T. Doles, G. Hribar, N. Furlan, A. Podgornik, Characterization of membrane adsorbers used for impurity removal during the continuous purification of monoclonal antibodies, J. Chromatogr. A. 1609 (2020), 460518, https://doi.org/10.1016/J.CHROMA.2019.460518.

[25] J. Labanda, J. Sabaté, J. Llorens, Modeling of the dynamic adsorption of an anionic dye through ion-exchange membrane adsorber, J. Memb. Sci. 340 (2009) 234–240, https://doi.org/10.1016/J.MEMSCI.2009.05.036.

[26] K. O'Donnell, S. Krishnathu, R. Bhatia, Z. Huang, W. Kelly, Evaluation of two-species binding model with anion-exchange membrane chromatography to predict pressure buildup during recovery of virus, Chem. Eng. Sci. 237 (2021), 116535, https://doi.org/10.1016/J.CES.2021.116535.

[27] C. Ladd Effio, T. Hahn, J. Seiler, S.A. Oelmeier, I. Asen, C. Silberer, L. Villain, J. Hubbuch, Modeling and simulation of anion-exchange membrane chromatography for purification of Sf9 insect cell-derived virus-like particles, J. Chromatogr. A. 1429 (2016) 142–154, https://doi.org/10.1016/J.CHROMA.2015.12.006.

[28] C. Boi, S. Dimartino, G.C. Sarti, Modelling and simulation of affinity membrane adsorption, J. Chromatogr. A. 1162 (2007) 24–33, https://doi.org/10.1016/J.CHROMA.2007.02.008.

[29] J. Labanda, J. Sabaté, J. Llorens, Experimental and modeling study of the adsorption of single and binary dye solutions with an ion-exchange membrane adsorber, Chem. Eng. J. 166 (2011) 536–543, https://doi.org/10.1016/J.CEJ.2010.11.013.

[30] E.R. Kenawy, A.A. Ghfar, S.M. Wabaidur, M.A. Khan, M.R. Siddiqui, Z. A. Alothman, A.A. Alqadami, M. Hamid, Cetyltrimethylammonium bromide intercalated and branched polyhydroxystyrene functionalized montmorillonite clay to sequester cationic dyes, J. Environ. Manage. 219 (2018) 285–293, https://doi.org/10.1016/J.JENVMAN.2018.04.121.

[31] M.A. Khan, S.M. Wabaidur, M.R. Siddiqui, A.A. Alqadami, A.H. Khan, Silico-manganese fumes waste encapsulated cryogenic alginate beads for aqueous environment de-colorization, J. Clean. Prod. 244 (2020), 118867, https://doi.org/10.1016/J.JCLEPRO.2019.118867.

[32] M. Zabihi, M. Omidvar, A. Motavalizadehkakhky, R. Zhiani, Competitive adsorption of arsenic and mercury on nano-magnetic activated carbons derived from hazelnut shell, Korean J. Chem. Eng. 39 (2022) 367–376, https://doi.org/10.1007/s11814-021-0903-4.

[33] S.Y. Suen, M.R. Etzel, A mathematical analysis of affinity membrane bioseparations, Chem. Eng. Sci. 47 (1992) 1355–1364, https://doi.org/10.1016/0009-2509(92)80281-G.

[34] J. Thömmes, M.-R. Kula, Membrane chromatography—an integrative concept in the downstream processing of proteins, Biotechnol. Prog. 11 (1995) 357–367, https://doi.org/10.1021/bp00034a001.

[35] S.Y. Suen, M. Caracotsios, M.R. Etzel, Sorption kinetics and axial diffusion in binary-solute affinity-membrane bioseparations, Chem. Eng. Sci. 48 (1993) 1801–1812, https://doi.org/10.1016/0009-2509(93)80350-Y.

[36] S.Y. Suen, M.R. Etzel, Sorption kinetics and breakthrough curves for pepsin and chymosin using pepstatin A affinity membranes, J. Chromatogr. A. 686 (1994) 179–192, https://doi.org/10.1016/0021-9673(94)00701-2.

[37] W. Hayduk, H. Laudie, Prediction of diffusion coefficients for nonelectrolytes in dilute aqueous solutions, AIChE J. 20 (1974) 611–615.

[38] I. Tatárová, P. Dreveňák, A. Kosior, M. Polakovič, Equilibrium and kinetics of protein binding on ion-exchange cellulose membranes with grafted polymer layer, Chem. Pap. 67 (2013) 1527–1536, https://doi.org/10.2478/s11696-012-0269-5.

[39] F. Benavente, R. Pero-Gascon, L. Pont, J. Jaumot, J. Barbosa, V. Sanz-Nebot, Identification of antihypertensive peptides in nutraceuticals by capillary electrophoresis-mass spectrometry, J. Chromatogr. A. 1579 (2018) 129–137, https://doi.org/10.1016/J.CHROMA.2018.10.018.

[40] F. Yan, Y. Chu, K. Zhang, F. Zhang, N. Bhandari, G. Ruan, Z. Dai, Y. Liu, Z. Zhang, A.T. Kan, M.B. Tomson, Determination of adsorption isotherm parameters with correlated errors by measurement error models, Chem. Eng. J. 281 (2015) 921–930, https://doi.org/10.1016/J.CEJ.2015.07.021.

[41] T. Andrea Osmari, R. Gallon, M. Schwaab, E. Barbosa-Coutinho, J. Baptista Severo Jr, J. Carlos Pinto, Statistical analysis of linear and non-linear regression for the estimation of adsorption isotherm parameters, 2013.

[42] V.C. Srivastava, I.D. Mall, I.M. Mishra, Equilibrium modelling of single and binary adsorption of cadmium and nickel onto bagasse fly ash, Chem. Eng. J. 117 (2006) 79–91, https://doi.org/10.1016/j.cej.2005.11.021.

[43] V.C. Srivastava, I.D. Mall, I.M. Mishra, Removal of cadmium(II) and zinc(II) metal ions from binary aqueous solution by rice husk ash, Colloids Surfaces A Physicochem. Eng. Asp. 312 (2008) 172–184, https://doi.org/10.1016/j.colsurfa.2007.06.048.

[44] E. Padilla-Ortega, R. Leyva-Ramos, J.V. Flores-Cano, Binary adsorption of heavy metals from aqueous solution onto natural clays, Chem. Eng. J. 225 (2013) 535–546, https://doi.org/10.1016/j.cej.2013.04.011.
[45] C. Teepakorn, K. Fiaty, C. Charcosset, Optimization of lactoferrin and bovine serum albumin separation using ion-exchange membrane chromatography, Sep. Purif. Technol. 151 (2015) 292–302, https://doi.org/10.1016/J.SEPPUR.2015.07.046.
[46] T. Gu, Mathematical modeling and scale-up of liquid chromatography: With application examples, second edition, Math. Model. Scale-Up Liq. Chromatogr. With Appl. Examples, Second Ed., 2015, pp. 1–207, 10.1007/978-3-319-16145-7/COVER.
[47] S.O. Rastegar, T. Gu, Empirical correlations for axial dispersion coefficient and Peclet number in fixed-bed columns, J. Chromatogr. A. 1490 (2017) 133–137, https://doi.org/10.1016/J.CHROMA.2017.02.026.
[48] A.A. Alqadami, M. Naushad, M.A. Abdalla, T. Ahamad, Z. Abdullah ALOthman, S. M. Alshehri, A.A. Ghfar, Efficient removal of toxic metal ions from wastewater using a recyclable nanocomposite: a study of adsorption parameters and interaction mechanism, J. Clean. Prod. 156 (2017) 426–436, https://doi.org/10.1016/J.JCLEPRO.2017.04.085.
[49] Z.A. Alothman, A.H. Bahkali, M.A. Khiyami, S.M. Alfadul, S.M. Wabaidur, M. Alam, B.Z. Alfarhan, Low cost biosorbents from fungi for heavy metals removal from wastewater, Sep. Sci. Technol. 55 (2020) 1766–1775, https://doi.org/10.1080/01496395.2019.1608242.
[50] Q. Hu, D. Wang, S. Pang, L. Xu, Prediction of breakthrough curves for multicomponent adsorption in a fixed-bed column using logistic and Gompertz functions, Arab. J. Chem. 15 (2022), 104034, https://doi.org/10.1016/J.ARABJC.2022.104034.